Stepping Toward Standard Methods of Small-Signal Parameter Extraction for HBT's

Mohammad Sotoodeh, Lucia Sozzi, Alessandro Vinay, A. H. Khalid, Zhirun Hu, Ali A. Rezazadeh, *Member, IEEE*, and Roberto Menozzi

***Abstract*—An improved HBT small-signal parameter extraction procedure is presented in which all the equivalent circuit elements are extracted analytically without reference to numerical optimization. Approximations required for simplified formulae used in the extraction routine are revised, and it is shown that the present method has a wide range of applicability, which makes it appropriate for GaAs- and InP-based single and double HBT's. Additionally, a new method is developed to extract the total delay time of HBT's at low frequencies, without the need to measure h_{21} at very high frequencies and/or extrapolate it with -20 dB/dec roll-off. The existing methods of finding the forward transit time are also modified to improve the accuracy of this parameter and its components. The present technique of parameter extraction and delay time analysis is applied to an InGaP/GaAs DHBT and it is shown that: 1) variations of all the extracted parameters are physically justifiable; 2) the agreement between the measured and simulated S- and Z-parameters in the entire range of frequency is excellent; and 3) an optimization step following the analytical extraction procedure is not necessary. Therefore, we believe that the present technique can be used as a standard extraction routine applicable to various types of HBT's.**

***Index Terms*—Delay times, equivalent circuits, forward transit time, heterojunction bipolar transistors, parameter extraction, small-signal, III–V compound semiconductors.**

I. Introduction

HETEROJUNCTION bipolar transistors (HBT's) based on III–V material systems are very attractive candidates for digital, analog, and power applications due to their excellent switching speed combined with high current driving capability [1], [2]. In that respect, there has long been a strong competition between III–V HBT's and their FET counterparts (MESFET and HEMT).

As the range of HBT's applicability constantly widens, the need for accurate small- and large-signal models is a key factor for successful employment of these devices in systems. The most commonly used small-signal parameter extraction technique is numerical optimization of the model generated S-parameters to fit the measured data. It is well known, however, that optimization techniques may result in nonphysical and/or nonunique values of the components. Also the optimized parameters are largely dependent on the initial values of the optimization process. Alternative extraction methods which ensure unique determination of as many equivalent circuit elements as possible are therefore of considerable importance. Several approaches for a more accurate and more physical parameter extraction are suggested in the literature. Costa *et al.* [3] have used several test structures to systematically de-embed the intrinsic HBT from its surrounding extrinsic and parasitic elements. However, this method requires three test structures for each device size on the wafer, ignores the nonuniformity across the wafer, and may involve an additional processing mask in some self-aligned technologies. Pehlke and Pavlidis [4] developed an analytic approach to extract the T-shaped equivalent circuit elements of HBT's. But this method, though attractive in many aspects, had two major disadvantages. First, the method was still relying on optimization to find the parameters of the emitter branch and elements of the delay time, a problem which was later resolved in [5]. Second, the distributed nature of the base resistance and base-collector capacitance was not taken into account. This last assumption, which was later addressed by many other authors, may result in a negative collector series resistance [6] or a nonphysical frequency behavior of the calculated emitter block [7].

Since 1992, other approaches were proposed, which took the distributed nature of $R_{\rm bb}$ and $C_{\rm bc}$ into account. The approach in [8] involves some unjustifiable assumptions (e.g., $\omega^2 C_{{\rm bc}\,i}^2 R_{{\rm bc}\,i} R_{{\rm bb}\,i} \gg 1$; see Fig. 1 for interpretation of the parameters), and some of the parameters are left to be obtained using numerical optimization and/or physical estimation. The same is almost true for the approach used by Schaper and Holzapfl [9], where it is assumed that $C_{{\rm bc}\,i} \ll C_{{\rm bc}\,x}$ and $R_{\rm be}^2 C_{\rm be} \gg L_e$. Rios *et al.* [10] proposed an attractive method in which maximum amount of information, parameter values, and constraints are extracted in order to minimize the number of unknown parameters to be evaluated by a final numerical optimization process. Kameyama *et al.* [11] used a similar approach to extract the equivalent circuit elements of a pnp HBT, but they claimed that their method can be applied to npn HBT's with a little modification. Measurement of S-parameters under open-collector condition is used in [6] to assist in finding the extrinsic series elements of the T-equivalent circuit, although nonlinear extrapolation has to be used in order to find the series elements (see [6, Fig. 2]). Additionally, all of the extrinsic series elements are assumed bias-independent. Finally, Samelis and Pavlidis [7] applied a novel impedance block conditioned optimization. This method seems rather involved in terms of

Manuscript received August 3, 1999; revised February 9, 2000. This work was supported by the U.K. Engineering and Physical Sciences Research Council (EPSRC). The review of this paper was arranged by Editor A. S. Brown.

M. Sotoodeh, L. Sozzi, A. H. Khalid, Z. Hu, and A. A. Rezazadeh are with the Department of Electronic Engineering, King's College London, London WC2R 2LS, UK (e-mail: ali.rezazadeh@kcl.ac.uk).

A. Vinay and R. Menozzi are with the Department of Information Engineering, University of Parma, Parma, Italy.

Publisher Item Identifier S 0018-9383(00)04245-3.

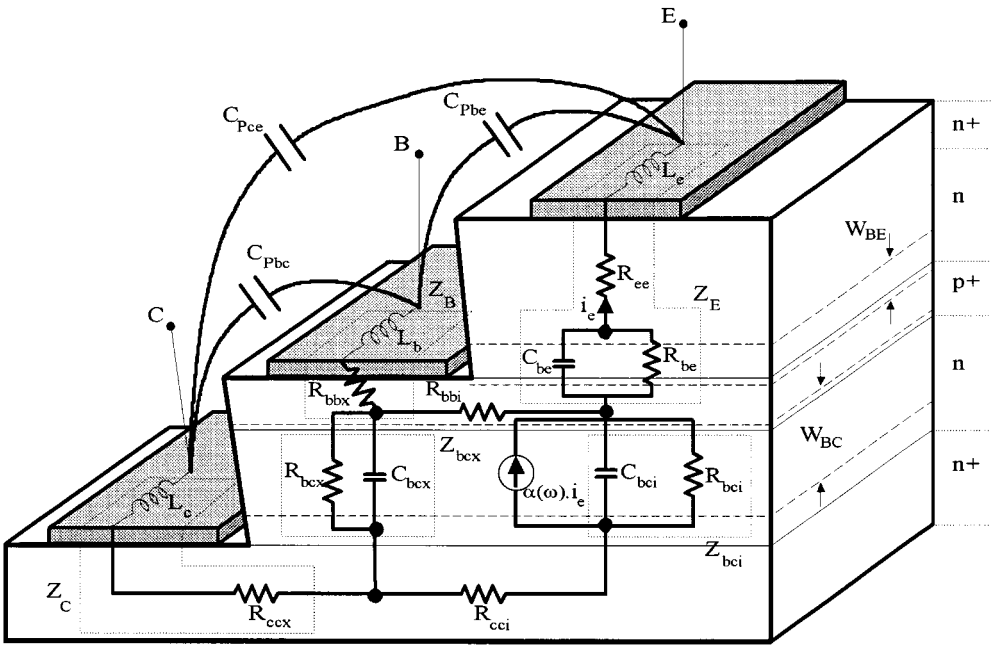

Fig. 1. Schematic cross-section of a small-geometry HBT together with its lumped element small-signal equivalent circuit. The impedance blocks defined in (A3)–(A7) are placed inside dashed boxes.

implementation and computation time, but otherwise has the advantage of preserving the physical structure of the impedance blocks.

From the brief review of the above works, it is clear that there is still a lack of a standard direct technique for small-signal parameter extraction of HBT's, although several positive steps have been taken. This is in contrast to FET parameter extraction that has for long benefited from a standard method [12], [13]. Therefore, it is necessary to review the existing methods and develop a straightforward and reliable small-signal parameter extraction technique with very reasonable assumptions that make it applicable to various types of HBT's.

Recently, Li and Prasad discussed the basic expressions and approximations used in small-signal parameter extraction of HBT's [14]. Based on this, they developed a procedure which was successfully applied to extract the parameters of an AlGaAs/GaAs HBT with emitter area of 30 μm^2 [15]. We believe that the Li and Prasad's work with some modifications, to be discussed in the present article, can be the basis for a standard method applicable to a wide range of HBT's. The modifications to [14] and [15] include different plotting and/or interpretation of the measured data, less restrictive assumptions, removing the necessity of a final optimization process, more general formulation of the common-base current gain, a different use of "cold-HBT" data, and physical explanation of some of the observed variations (which could not be explained in [15]). These modifications are clearly addressed in the forthcoming sections.

In addition, new methods are introduced to obtain the total delay time $(\tau_{\rm EC})$ and the forward transit time $(\tau_F \equiv \tau_B + \tau_C)$ from the measured Z-parameters at low frequencies, without the requirement of extrapolating h_{21} at higher frequency region.

The structure of this paper is as follows. Section II describes the theoretical approximations of Z-parameters, assumptions made, and the range of their applicability. Then in Section III, a parameter extraction technique based on the results of Section II will be developed. Section IV is devoted to the new methods of finding total delay time and forward transit time from the measured Z-parameters at low frequencies. Discussion of the results in Section V will be finally followed by main conclusions of this work in Section VI.

II. Z-Parameters Formulation and Approximations

Fig. 1 shows the schematic diagram of an npn HBT together with its associated small-signal lumped-element equivalent circuit. This is a T-shaped equivalent circuit with three added parallel capacitances due to the contact pads. Since the T-shaped equivalent circuit is more closely related to the original derivation of the common-base Y-parameters of bipolar transistors [16], [17] and involves less simplifying assumptions than the π-equivalent circuit, it is usually employed in the literature (and in the present work) for the purpose of small-signal parameter extraction of HBT's. The distributed nature of the base resistance and the base-collector capacitance is modeled in this diagram by dividing them into only two sub-elements; namely intrinsic and extrinsic parts. Division of these elements into more sub-regions is discussed in, e.g., [18], [19], but one has to mainly rely on optimization techniques to evaluate the extra elements.

One feature in common among different methods of parameter extraction in the literature is that first the parasitic pad capacitances are determined. Measurement of an open test structure [3], and variation of the measured total capacitances at low frequencies with reverse bias [18] or with junction area [20] are proposed to distinguish between the junction and parasitic capacitances. Once the parasitic pad capacitances are determined, the internal device will be de-embedded from these using standard network parameter transformation. Usually, the

subcollector of HBT's is at least three to five times thicker than their base region. Therefore, $R_{\mathrm{cc}\,i}$ is a very small resistance, especially in npn III–V HBT's where the much higher mobility for electrons is also responsible for a negligible $R_{\mathrm{cc}\,i}$. Consequently, one can merge the effects of $R_{\mathrm{cc}\,i}$ and $R_{\mathrm{cc}\,x}$ into a single resistance R_{cc} connected in series with the collector inductance L_c. The resultant equivalent circuit, after de-embedding the pad capacitances, can be explained by a set of Z-parameters. The formulation of Z-parameters in the present work is similar to that in [14], and is repeated for readers' convenience in the Appendix. It is important to note that more physically complete equations for $\alpha(\omega)$ and C_{be}, as compared to those in [14], are used here. Also reverse-biased B/C junction resistances are considered for both the intrinsic and extrinsic parts. We further define:

$$R_{\mathrm{bc}} \equiv (1/R_{\mathrm{bc}\,i} + 1/R_{\mathrm{bc}\,x})^{-1} \tag{1}$$

$$C_{\mathrm{bc}} \equiv C_{\mathrm{bc}\,i} + C_{\mathrm{bc}\,x} \tag{2}$$

$$r \equiv C_{\mathrm{bc}\,i}/C_{\mathrm{bc}} \tag{3}$$

If one assumes

$$R_{\mathrm{bb}\,i} \ll R_{\mathrm{bc}} \tag{4}$$

$$[\omega C_{\mathrm{bc}} r(1-r) R_{\mathrm{bb}\,i}]^2 \ll 1 \tag{5}$$

$$(\omega C_{\mathrm{bc}} R_{\mathrm{bc}})^2 \gg 1 \tag{6}$$

then after some algebraic manipulation one can arrive at the following simplified equations:

$$Z_{11} - Z_{12} \approx R_{\mathrm{bb}\,x} + rR_{\mathrm{bb}\,i} + j\omega[L_b - r^2(1-r)R_{\mathrm{bb}\,i}^2 C_{\mathrm{bc}}] + \frac{jR_{\mathrm{bb}\,i}}{\omega C_{\mathrm{bc}}}\left(\frac{r}{R_{\mathrm{bc}\,x}} - \frac{1-r}{R_{\mathrm{bc}\,i}}\right) \tag{7}$$

$$Z_{22} - Z_{21} \approx R_{\mathrm{cc}} - r(1-r)R_{\mathrm{bb}\,i} + \frac{1}{\omega^2 C_{\mathrm{bc}}^2 R_{\mathrm{bc}}} + j\omega L_c - \frac{j}{\omega C_{\mathrm{bc}}}. \tag{8}$$

It is worth pointing out that assumptions (5) and (6) are second-order approximations, as opposed to first-order approximations suggested in [14] for the intermediate frequency range (e.g., $\omega C_{\mathrm{bc}\,i} R_{\mathrm{bb}\,i}$ and $\omega C_{\mathrm{bc}\,x} R_{\mathrm{bb}\,i} \ll 1$). This makes the range for applicability of (4)–(8) wider. If, for instance, "$\ll$" means "at least ten times smaller", then with some rather conservative values of $R_{\mathrm{bc}} = 10\ \mathrm{k}\Omega$, $R_{\mathrm{bb}\,i} = 20\ \Omega$, $r = 0.5$, and $C_{\mathrm{bc}} = 100 - 200$ fF, the above approximations would be valid for $0.5\ \mathrm{GHz} \le f \le 50$ GHz. Therefore, even in InP/InGaAs HBT's where $R_{\mathrm{bb}\,i}$ is two to three times larger than GaAs-based HBT's, there would be a wide enough frequency range over which (4)–(8) are valid and small-signal parameters can be extracted using the technique discussed in this work. Another result of the above discussion is that extremely low frequency range (characterized by $\omega C_{\mathrm{bc}} R_{\mathrm{bc}} \ll 1$) and extremely high frequency range (characterized by $\omega C_{\mathrm{bc}} R_{\mathrm{bb}\,i} \gg 1$) as defined in [14] require measurement frequencies as low as 50 MHz or as high as 500 GHz, which can not be achieved using presently available network analyzers.

Other useful relations that can be directly (without any assumption) derived from (A1) and (A2) are

$$\alpha = \frac{Z_{12} - Z_{21}}{Z_{22} - Z_{21} - Z_C} \tag{9}$$

$$\begin{aligned} Z_E &= Z_{12} - \frac{(1-\alpha)R_{\mathrm{bb}\,i} Z_{\mathrm{bc}\,x}}{R_{\mathrm{bb}\,i} + Z_{\mathrm{bc}\,i} + Z_{\mathrm{bc}\,x}} \cdot \frac{Z_{\mathrm{bc}\,i}}{Z_{\mathrm{bc}\,x}} \\ &= Z_{12} - (1-\alpha)(Z_{11} - Z_{12} - Z_B) \cdot \frac{Z_{\mathrm{bc}\,i}}{Z_{\mathrm{bc}\,x}} \\ &= Z_{12} - \frac{(Z_{22} - Z_{12} - Z_C)(Z_{11} - Z_{12} - Z_B)}{Z_{22} - Z_{21} - Z_C} \cdot \frac{Z_{\mathrm{bc}\,i}}{Z_{\mathrm{bc}\,x}}. \end{aligned} \tag{10}$$

Therefore, if Z_C, Z_B, and $(Z_{\mathrm{bc}\,i}/Z_{\mathrm{bc}\,x})$ are known, Z_E can be accurately determined. However as will be shown in the next section, elements of Z_E can be determined at low frequencies without accurate knowledge of the above impedance blocks.

Under forward active mode of operation, and especially at high current regime, the assumption:

$$(\omega C_{\mathrm{be}} R_{\mathrm{be}})^2 \ll 1 \tag{11}$$

would be valid in a wide frequency range and (A5) can be approximated as

$$Z_E \approx R_{\mathrm{ee}} + R_{\mathrm{be}} + j\omega\left(L_e - R_{\mathrm{be}}^2 C_{\mathrm{be}}\right). \tag{12}$$

"Cold" condition for HBT's is defined as the condition when both junctions are zero-biased (or reverse-biased). Under such condition, dc current is zero, hence α would be extremely small and the device behaves like a passive component ($Z_{21} = Z_{12}$). Expressions (4)–(8) would still be valid. Also (A9) simplifies to $C_{\mathrm{be}} \approx C_{j\,\mathrm{be}}$. Additionally, R_{be} is very large and (11)–(12) are no longer valid. Instead, assuming $(\omega C_{j\,\mathrm{be}} R_{\mathrm{be}})^2 \gg 1$ and (4)–(6), one can write

$$\begin{aligned} Z_{12}(\mathrm{cold}) &= Z_{21}(\mathrm{cold}) \\ &= R_{\mathrm{ee}} + (1-r)R_{\mathrm{bb}\,i} + \frac{1}{\omega^2 C_{j\,\mathrm{be}}^2 R_{\mathrm{be}}} \\ &\quad + j\omega\left[L_e - r(1-r)^2 R_{\mathrm{bb}\,i}^2 C_{\mathrm{bc}}\right] - \frac{j}{\omega C_{j\,\mathrm{be}}} \\ &\quad + \frac{jR_{\mathrm{bb}\,i}}{\omega C_{\mathrm{bc}}}\left(\frac{1-r}{R_{\mathrm{bc}\,i}} - \frac{r}{R_{\mathrm{bc}\,x}}\right). \end{aligned} \tag{13}$$

As will be shown in the next section $(1-r)/R_{\mathrm{bc}\,i} \approx r/R_{\mathrm{bc}\,x}$, and therefore, the last terms on the right-hand-side of (7) and (13) are extremely small and can be ignored.

III. Parameter Extraction Technique

In this section, an improved version of the technique explained in [15] will be applied to extract the small-signal parameters of an InGaP/GaAs double HBT with $(3\times10)\times4\ \mu\mathrm{m}^2$ B/E area (accounting for the estimated mesa undercut) and $32\times10\ \mu\mathrm{m}^2$ B/C area. The intrinsic part of the layer structure of this DHBT consists of 1000 Å $n = 3\times10^{17}$ cm^{-3} InGaP emitter, 1000 Å p$^+$ $= 3\times10^{19}$ cm^{-3} GaAs base, 200 Å $n = 1\times10^{16}$ cm^{-3} GaAs spacer, and 4800 Å 6×10^{16} cm^{-3} InGaP collector, all grown on semi-insulating GaAs substrate. Device fabrication is discussed elsewhere [21]. DC

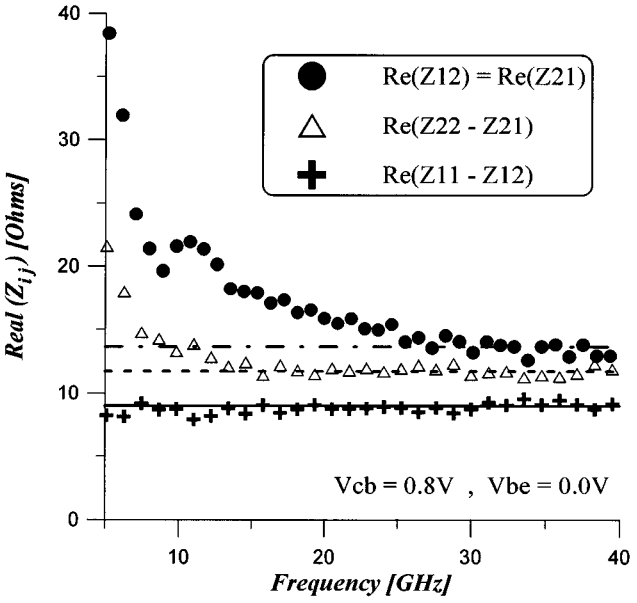

Fig. 2. Real parts of the Z-parameters as a function of frequency obtained under cold-HBT condition.

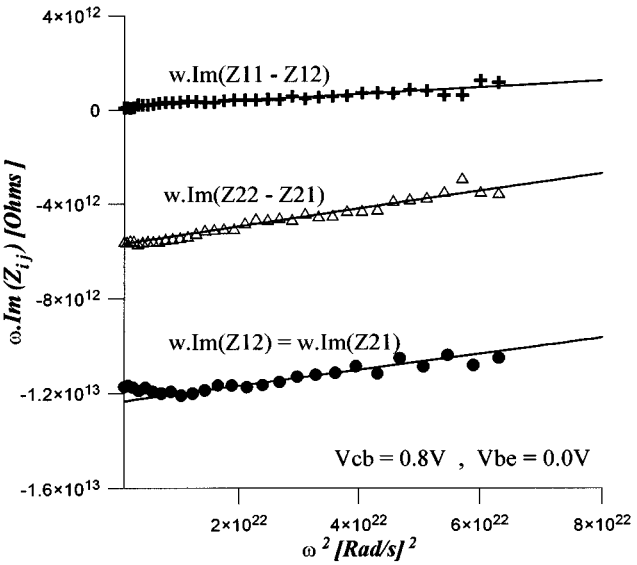

Fig. 3. Plot of $\omega \cdot \mathrm{Im}(Z_{ij})$ versus ω^2 under cold-HBT condition.

characterization of the device is carried out using HP4145B Semiconductor Parameter Analyzer. Then the S- parameters are measured on-wafer using HP8510 Network Analyzer and Cascade Microtech RF probes in the frequency range 100 MHz to 40 GHz.

Small-signal parameter extraction starts from de-embedding the internal device from parasitic pad capacitances surrounding it. Then, a series of S-parameter measurements is carried out under constant V_{cb} and variable collector current (including $I_c = 0$, i.e., the cold-HBT). The cold-HBT measurement is to assist in finding $R_{\mathrm{bb}\,x}$, which is assumed bias-independent, as well as C_{Pce}. Measured data under variable I_c will be used to separate current-dependent elements from those insensitive to current.

As to the measurement of the parasitic pad capacitances, we employed a combination of two methods. First method is measurement of an open test structure. Second is the variation of reverse bias across B/E and B/C junctions of a cold-HBT to distinguish between the junction and parasitic capacitances [18]. Both methods resulted in similar values of C_{Pbc} and C_{Pce}, but C_{Pbe} obtained from the second method was significantly larger than that from the first. We believe that this is due to the full depletion of the emitter n-region under reverse bias condition which results in a misinterpretation of the variation of the total measured capacitance with bias. Therefore, we suggest to use C_{Pbe} and C_{Pbc} measured from an open test structure, and only C_{Pce} from the second method. This way, one avoids the extra measurements of the cold-HBT at variable reverse biases; only one cold-HBT measurement is required to find C_{Pce}, which has to be carried out for the purpose of extracting $R_{\mathrm{bb}\,x}$ anyway.

Once the pad capacitances are determined, the internal device can be de-embedded from them. Next, one should obtain maximum amount of information from measured cold-HBT results. In this analysis, we will have the following additional assumptions which all seem physically justifiable: 1) $R_{\mathrm{bb}\,x}$ is assumed bias independent, 2) R_{ee} is constant at low current levels, but it may change at higher currents, and 3) $r = (B/E \text{ area})/(B/C \text{ area})$ only under low current injection condition; it may change at higher levels of current. It is quite clear that the above assumptions are much less restrictive than those in [15]. In [15] it is assumed that all the extrinsic series elements ($L_e, L_b, L_c, R_{\mathrm{ee}}, R_{\mathrm{cc}}$, and $R_{\mathrm{bb}\,x}$) and $C_{\mathrm{bc}\,x}$ are absolutely bias-independent, while this is not required in the present work.

As seen from (7), (8), and (13), at high frequencies under cold condition the real parts of $(Z_{11} - Z_{12})$, $(Z_{22} - Z_{21})$, and Z_{12} saturate at $[R_{\mathrm{bb}\,x} + rR_{\mathrm{bb}\,i}]$, $[R_{\mathrm{cc}} - r(1-r)R_{\mathrm{bb}\,i}]$, and $[R_{\mathrm{ee}} + (1-r)R_{\mathrm{bb}\,i}]$, respectively (see Fig. 2). In case any of the real parts is not completely saturating at high frequencies, one can plot it versus $(1/\omega^2)$ then fit a straight line through the data points and extrapolate to the y-intercept. Since r at low currents is equal to the area ratio between the B/E and B/C junctions, one has a system of three equations and four unknowns, namely $R_{\mathrm{bb}\,i}$, $R_{\mathrm{bb}\,x}$, R_{ee}, and R_{cc}. Our approach to find these elements is to assume a reasonable value for R_{ee}, which, for instance, can be obtained from dc open collector measurement [22]. It is important to mention that the above value of R_{ee} only serves as an initial guess and it will be corrected in one of the early stages of parameter extraction for hot-HBT, after which only one or maximum two iterations will result in converging values of all the series resistive elements. Once R_{ee} is known, the other three resistances can be found, but only $R_{\mathrm{bb}\,x}$ will be assumed constant and fed into the parameter extraction procedure for hot-HBT.

Although the information obtained from imaginary parts of the Z-parameters measured under cold condition is not required for the parameter extraction of hot-HBT, it is constructive to show the variation of $\mathrm{Im}(Z_{ij})$ to confirm the validity of (7), (8), and (13). Fig. 3 shows a plot of $\omega \cdot \mathrm{Im}(Z_{11} - Z_{12})$, $\omega \cdot \mathrm{Im}(Z_{22} - Z_{21})$, and $\omega \cdot \mathrm{Im}(Z_{12})$ versus ω^2. Linear variation of these plots confirms, once again, the validity of the approximations used to derive (7), (8), and (13). The y-intercept of the plots are ~ 0, $-1/C_{\mathrm{bc}}$, and $-1/C_{j\,\mathrm{be}}$, respectively. A zero y-intercept for the plot of $\omega \cdot \mathrm{Im}(Z_{11} - Z_{12})$ versus ω^2 supports the earlier statement that the last terms in (7) and (13) are indeed very small.

Next the S-parameters of the device under forward active mode with variable I_c and constant $V_{\rm cb}$ (=0.8 V in this case) will be measured. The reason for having a constant $V_{\rm cb}$ rather than a constant $V_{\rm ce}$ will be clarified later. Bearing in mind that (7) and (8) are still valid under hot-HBT condition, one can obtain the values of $[R_{{\rm bb}x} + rR_{{\rm bb}i}]$, $[R_{\rm cc} - r(1-r)R_{{\rm bb}i}]$, $[L_b - r^2(1-r)R^2_{{\rm bb}i}C_{\rm bc}]$, $C_{\rm bc}$, and L_c by plotting real parts of $(Z_{11}-Z_{12})$ and $(Z_{22}-Z_{21})$ versus f, and $\omega\cdot{\rm Im}(Z_{11}-Z_{12})$ and $\omega\cdot{\rm Im}(Z_{22}-Z_{21})$ versus ω^2. Since $R_{{\rm bb}x}$ is known from cold results, $R_{{\rm bb}i}$ can be determined and consequently $R_{\rm cc}$ and L_b are evaluated. In [15], after $C_{\rm bc}$ is obtained, L_c is determined from $\omega^{-1}\cdot[{\rm Im}(Z_{22}-Z_{21}) + 1/(\omega C_{\rm bc})]$ and it is stated that this parameter is very much sensitive to the value of $C_{\rm bc}$. But in the present method $C_{\rm bc}$ and L_c are obtained independently from y-intercept and gradient of the plot of $\omega\cdot{\rm Im}(Z_{22}-Z_{21})$ versus ω^2, respectively.

If ${\rm Re}(Z_{22}-Z_{21})$ is plotted against $1/\omega^2$, the gradient of the fitted line will be equal to $1/(R_{\rm bc}C^2_{\rm bc})$. Since $C_{\rm bc}$ is known, $R_{\rm bc}$ can be determined. If $R_{\rm bc}$ is extremely large, then the term $1/(\omega^2 C^2_{\rm bc}R_{\rm bc})$ would be negligibly small and almost comparable to the terms already neglected in the derivation of (8). Therefore, the plot of ${\rm Re}(Z_{22}-Z_{21})$ versus $1/\omega^2$ may result in a nonlinear variation or even a negative slope. In such circumstances, one can use a large value for $R_{\rm bc}$ bearing in mind that this element does not affect the small-signal parameters significantly. As to the determination of $R_{{\rm bc}i}$ and $R_{{\rm bc}x}$, one can consider the inverse dependence of resistance on area:

$$\frac{Z_{{\rm bc}i}}{Z_{{\rm bc}x}} = \frac{R_{{\rm bc}i}}{R_{{\rm bc}x}} = \frac{(B/C\ \text{area}) - (B/E\ \text{area})}{B/E\ \text{area}} = \frac{1-r}{r} \tag{14a}$$

$$R_{\rm bc} = rR_{{\rm bc}i} = (1-r)R_{{\rm bc}x} \tag{14b}$$

At this stage, all of the terms on the RHS of (9) and (10) are known, and therefore, α and Z_E can be evaluated. Variation of α with frequency will be discussed in the next section. As to the determination of Z_E, magnitude of $(1-\alpha)$ will become large at high frequencies. Consequently, any small error in the determination of Z_B, Z_C, or $(Z_{{\rm bc}i}/Z_{{\rm bc}x})$ may result in a significant deviation of Z_E at higher frequencies. But the effect of the above impedance blocks on Z_E is just minimal at lower range of frequency where $(1-\alpha)\approx 0$. Therefore, $(R_{\rm ee}+R_{\rm be})$ can be evaluated from the real part of RHS of (10) at low frequencies. Fig. 4 shows the variation of ${\rm Re}(Z_E)$ with frequency for different values of dc collector current. All of the plots in Fig. 4 saturate at low frequencies at $(R_{\rm ee}+R_{\rm be})$, and at higher frequencies asymptotically approach $R_{\rm ee}$, as expected from the formulation of Z_E in (A5) [7]. Determined values of $(R_{\rm ee}+R_{\rm be})$ can be plotted against $(1/I_c)$ to differentiate between $R_{\rm ee}$ and $R_{\rm be}$ (Fig. 5). The y-intercept of this plot gives a corrected $R_{\rm ee}$, which has to be used in order to obtain a corrected value of $R_{{\rm bb}x}$ through the cold-HBT measured resistances. $R_{\rm be} = \eta kT/qI_c$ can also be found from the gradient of the plot in Fig. 5, which gives an ideality factor, η, of 1.03. The sudden increase of $(R_{\rm ee}+R_{\rm be})$ at the highest current point is due to device self-heating which is known to increase both $R_{\rm ee}$ and $R_{\rm be}$ [23].

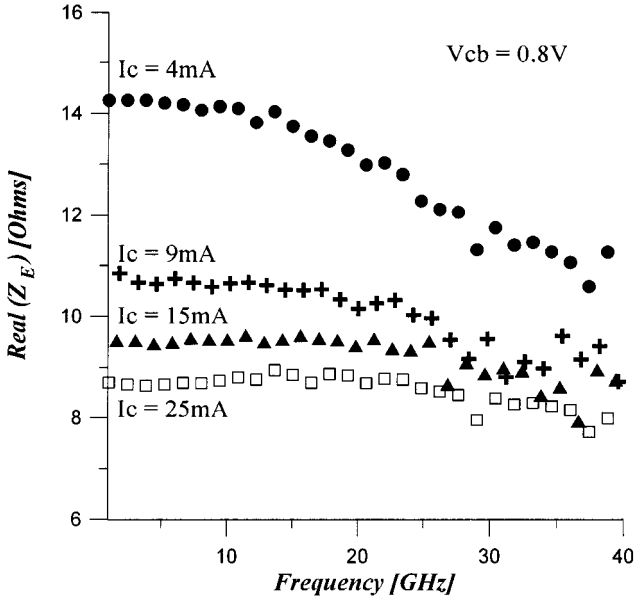

Fig. 4. Plots of ${\rm Real}(Z_E)$ versus frequency under variable I_c. All the curves saturate at low frequencies to the value of $(R_{\rm cc}+R_{\rm be})$.

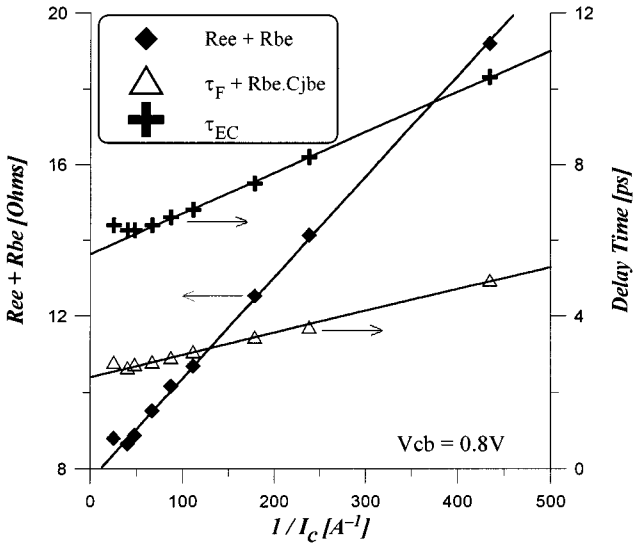

Fig. 5. Variation of $(R_{\rm cc}+R_{\rm be})$, $(\tau_F + R_{\rm bc}\times C_{j\,{\rm bc}})$, and $\tau_{\rm EC}$ as determined from Figs. 4, 7, and 8, respectively, with $(1/I_c)$. Extrapolated y-intercepts of the fitting lines give $R_{\rm cc}$, τ_F, and $\tau_F + (R_{\rm cc}+R_{\rm cc})C_{\rm bc}$, respectively.

Although any change in $R_{\rm ee}$ will be directly reflected to a change in $R_{{\rm bb}x}$, $R_{{\rm bb}i}$, and $R_{\rm cc}$ with more or less similar magnitude, the resultant variation of the latter parameters only has a minor effect on $R_{\rm ee}$ and $R_{\rm be}$, which are determined in the low frequency region where $(1-\alpha)\approx 0$. Therefore, the above procedure will be a very fast converging iteration with only one or two steps required. It is worth mentioning that in [15] $R_{{\rm bb}i}$, $R_{{\rm bb}x}$, and $R_{\rm cc}$ are determined by numerical optimization and/or using assumptions related to extremely high frequencies, while fully analytical methods in measurable range of frequency are employed in the present work.

Once the iteration procedure is converged, one can plot the imaginary part of Z_E versus ω to find $[L_e - R^2_{\rm be}C_{\rm be}]$ and thus L_e. Imaginary part of Z_E, obtained from the RHS of (10), is very much sensitive to the value of r. Therefore, an accurate

TABLE I
DIRECTLY EXTRACTED AND OPTIMIZED PARAMETERS UNDER VARIABLE COLLECTOR CURRENT AND CONSTANT V_{cb}, OF 0.80 V. THE RELATIVE ERRORS OF CALCULATION, AS DEFINED IN [15], ARE ALSO GIVEN

Extracted Cold HBT Data					
V_{cb} [V]	V_{be} [V]	$R_{ee}+(1-r)R_{bbi}$ [Ω]	$R_{bbx}+r.R_{bbi}$ [Ω]	$R_{cc}-r(1-r)R_{bbi}$ [Ω]	C_{bc} [fF]	C_{jbe} [fF]
0.80	0.00	13.66	8.96	11.72	175.2	81.2

Extracted Hot HBT Data										Optimized
I_c [mA]	2.3	4.2	5.6	9	11.5	15	21	25	40	9
r	0.376	0.371	0.372	0.371	0.369	0.365	0.356	0.349	0.345	0.349
C_{Pbc} [fF]	12.2									12.2
C_{Pbe} [fF]	20.0									20.0
C_{Pce} [fF]	53.9									55.5
R_{bbx} [Ω]	5.40									5.18
R_{ee} [Ω]	7.72								7.93	7.98
R_{bbi} [Ω]	9.36	9.18	9.08	8.82	8.32	7.50	6.47	6.27	6.26	9.59
R_{cc} [Ω]	12.13	11.95	11.97	11.74	11.37	11.02	10.81	10.81	11.96	11.67
R_{be} [Ω]	11.48	6.42	4.82	2.98	2.45	1.80	1.16	0.94	0.87	2.95
R_{bc} [Ω]	>50	>50	>50	43.2	32.7	27.1	24.3	21.9	21.3	44.1
C_{bc} [fF]	175.5	174.0	174.3	174.1	173.5	172.4	170.1	168.1	167.3	173.1
C_{jbe} [fF]	218									216.4
C_{be} [fF]	341	424	486	654	738	968	1389	1601	1741	660
L_b [pH]	25.9	26.1	25.4	26.1	26.1	26.8	27.7	25.1	27.2	26.1
L_c [pH]	31.9	32.2	30.1	31.2	34.8	35.8	36.2	33.0	36.1	31.2
L_e [pH]	28.6	27.0	25.2	25.6	26.7	26.6	26.2	26.8	30.1	25.6
α_0	.9835	.9837	.9850	.9863	.9866	.9871	.9872	.9873	.9860	.9863
τ_B [ps]	1.69	1.59	1.55	1.56	1.53	1.62	1.63	1.56	1.59	1.57
τ_C [ps]	0.77	0.72	0.85	0.86	0.86	0.80	0.86	0.90	0.98	0.86
τ_{EC} [ps]	10.33	8.20	7.51	6.81	6.61	6.40	6.27	6.26	6.40	6.98
τ_{EC} from h_{21} [ps]	9.85	7.90	7.24	6.63	6.44	6.28	6.19	6.17	6.29	—
relative error [%]	0.34	0.18	0.16	0.10	0.11	0.12	0.14	0.12	0.43	0.09

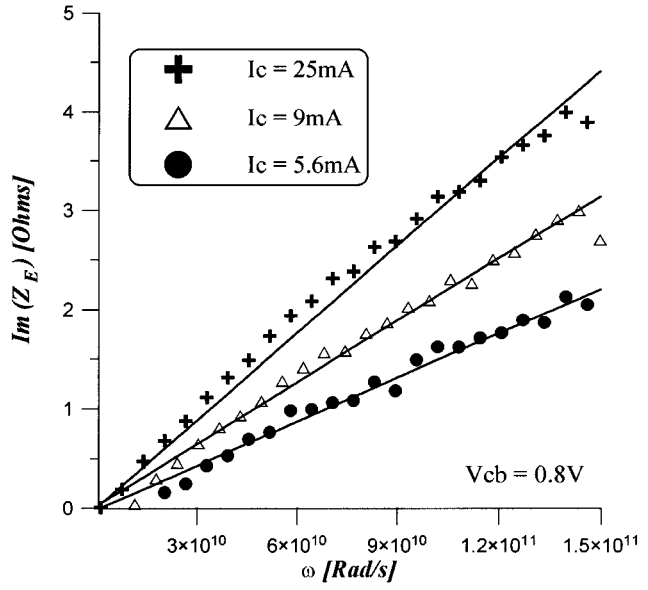

Fig. 6. $\mathrm{Im}(Z_E)$ versus ω under various collector current levels. The gradient of the fitting line is equal to $(L_e - R_{\mathrm{be}}^2 C_{\mathrm{be}})$.

value of r considering the undercutting of B/E and B/C junctions is crucial in determining L_e, otherwise one would observe a nonphysical saturating behavior for $\mathrm{Im}(Z_E)$. $[L_e - R_{\mathrm{be}}^2 C_{\mathrm{be}}]$ is an increasing function of I_c (see Fig. 6), but once corrected for the variation of $R_{\mathrm{be}}^2 C_{\mathrm{be}}$, shows an almost constant value of L_e versus collector current. Values of all the extracted parameters for the device under study with variable I_c and constant $V_{\mathrm{cb}} = 0.8$ V are summarized in Table I.

IV. DELAY TIME ANALYSIS

In the previous section, direct extraction of the parameter $\alpha(\omega)$ was explained using (9). The frequency dependence of this parameter includes sufficient information to extract α_0, τ_B, and τ_C. This is to be discussed in this section. Using (A8) given in the Appendix one can write

$$\frac{1}{|\alpha|^2} = \frac{(\omega\tau_C)^2}{\alpha_0^2 \cdot \sin^2(\omega\tau_C)} \cdot [1 + \omega^2 (m\tau_B + R_{\mathrm{be}} C_{j\,\mathrm{be}})^2]$$

Then, expanding the Taylor series of $\sin(\omega\tau_C)$ and ignoring the ω^4 terms (and higher powers of ω), the following equation can be derived:

$$\frac{1}{|\alpha|^2} \approx \frac{1 + \omega^2 \left[(m\tau_B + R_{\mathrm{be}} C_{j\,\mathrm{be}})^2 + \tau_C^2/3\right]}{\alpha_0^2}. \tag{15}$$

Therefore, α_0 and the term inside the square bracket in (15) can be extracted from the y-intercept and gradient of $1/|\alpha|^2$ versus ω^2. This plot is shown in Fig. 7 for the device under study at various collector current levels. A linear behavior can be observed in this plot for the low to medium frequency range.

If one further assumes

$$\omega^2 (m\tau_B + R_{\mathrm{be}} C_{j\,\mathrm{be}})^2 \ll 1 \tag{16a}$$

$$\omega^2 [(1-m)\tau_B + \tau_C]^2 \ll 1 \tag{16b}$$

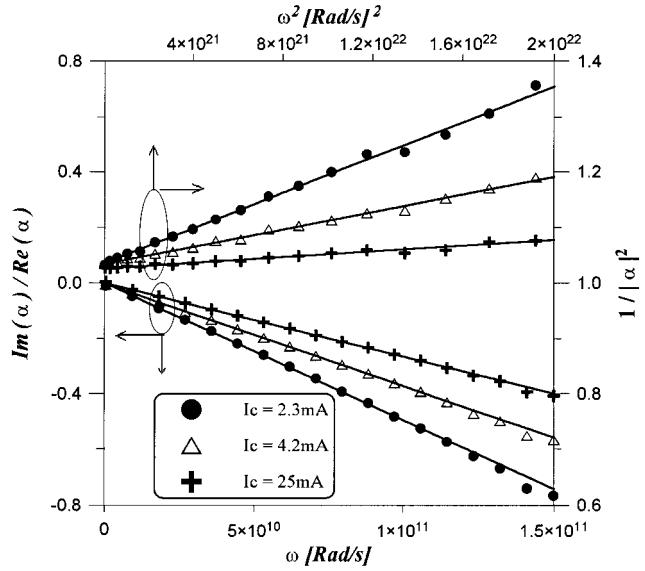

Fig. 7. Variation of $1/|\alpha|^2$ with ω^2, and $\mathrm{Im}(\alpha)/\mathrm{Re}(\alpha)$ with ω under various I_c levels.

then

$$\alpha \approx \frac{\alpha_0 \cdot \sin(\omega\tau_C)}{\omega\tau_C}[1 - j\omega(\tau_B + \tau_C + R_{\mathrm{be}}C_{j\,\mathrm{be}})]. \quad (17a)$$

$$\frac{1}{\alpha} \approx \frac{\omega\tau_C}{\alpha_0 \cdot \sin(\omega\tau_C)}[1 + j\omega(\tau_B + \tau_C + R_{\mathrm{be}}C_{j\,\mathrm{be}})] \quad (17b)$$

Therefore, $(\tau_B + \tau_C + R_{\mathrm{be}}C_{j\,\mathrm{be}})$ can be obtained from a plot of $\mathrm{Im}(1/\alpha)/\mathrm{Re}(1/\alpha) = -(\mathrm{Im}(\alpha)/\mathrm{Re}(\alpha))$ versus ω (Fig. 7). The values of $(\tau_B+\tau_C+R_{\mathrm{be}}C_{j\,\mathrm{be}})$ at various current levels are plotted against $(1/I_c)$ in Fig. 5. Since R_{be} is already known as a function of $(1/I_c)$, $C_{j\,\mathrm{be}}$ can be determined from the gradient of the above plot. This method assumes that $C_{j\,\mathrm{be}}$ does not vary significantly with slight changes of V_{be} in the current range considered. Linearity of this plot confirms that the latter assumption is a reasonable one. The obtained value of $C_{j\,\mathrm{be}}$ is $\sim$218 fF. The forward transit time, τ_F, can also be accurately evaluated from the y-intercept of the above plot. This method of characterizing the forward transit time is only relying on an accurate value of R_{cc}, which is to be used in (9) to find $\alpha(\omega)$; collector series inductance can be shown to have a negligible effect on α. Therefore, the present method is expected to be much more reliable than the conventional method of plotting total delay time, τ_{EC}, versus $(1/I_c)$, which additionally requires a prior knowledge of R_{ee} and C_{bc} (see (19) and Fig. 5). Also it is shown by Lee [24] that this method of determining τ_F is much less sensitive to errors in de-embedding pad capacitances. However, the method suggested by Lee [24], [25] is slightly different from the one used in the present work. Lee has suggested to use

$$\mathrm{Im}\left(\frac{Z_{22} - Z_{12} - Z_C}{Z_{12} - Z_{21}}\right) = \mathrm{Im}\left(\frac{1-\alpha}{\alpha}\right) = \mathrm{Im}\left(\frac{1}{\alpha}\right) \approx \tau_B + \tau_C + R_{\mathrm{be}}C_{j\,\mathrm{be}} \quad (18)$$

while the last approximate equality in (18) clearly ignores the term $\alpha_0 \cdot \sin(\omega\tau_C)/\omega\tau_C$ in (17). Therefore, the present method is expected to give more accurate results.

After finding $C_{j\,\mathrm{be}}$ from the plot in Fig. 5, the plots in Fig. 7 give us two equations for the two unknowns τ_B and τ_C. The method of extracting τ_B and τ_C in this work can be considered as a modified version of our previous work [5]. Finally, C_{be} can be evaluated using (A9). At this stage it must be pointed out that Li and Prasad [14], [15] used the invalid assumption of $C_{\mathrm{be}} \propto I_c$ (which ignores $C_{j\,\mathrm{be}}$) and a plot of $[L_e - R_{\mathrm{be}}^2 C_{\mathrm{be}}]$, obtained from Fig. 6, versus $(1/I_c)$ to find C_{be}. Therefore, they obtained a nonlinear plot (Fig. 13 in [15]) and an inaccurate value of C_{be} which necessitated numerical optimization. But even optimization is relatively insensitive to C_{be}, and hence, C_{be} could not be determined accurately in their work. This problem does not exist in the present work. Additionally, the formula for τ_B in [15] is incorrectly stated as $\tau_B = R_{\mathrm{be}}C_{\mathrm{be}}(=1/\omega_\alpha)$ and the term $\sin(\omega\tau_C)/(\omega\tau_C)$ is ignored in their $\alpha(\omega)$ expression. Based on these formulae, Li *et al.* observed values of τ_B which were unexpectedly varying with both I_b and V_{ce} (Tables II and III in [15]). In contrast, τ_B's obtained in the present work are almost constant with bias (1.61 ± 0.08 ps), since a physically correct formula for C_{be} [(A9)] is used here.

The total delay time in HBT's can be written as [26]:

$$\frac{1}{2\pi f_T} \equiv \tau_{\mathrm{EC}} = \tau_B + \tau_C + R_{\mathrm{be}}C_{j\,\mathrm{be}} + (R_{\mathrm{be}} + R_{\mathrm{ee}} + R_{\mathrm{cc}}) \cdot C_{\mathrm{bc}}. \quad (19)$$

The conventional method of finding the total delay time is to plot h_{21} versus frequency and extrapolate the graph with the slope -20 dB/dec (single-pole approximation for h_{21}) to locate the frequency, f_T, where h_{21} reaches 0 dB gain. However, h_{21} usually deviates from the -20 dB/dec roll-off due to the importance of higher order poles and zeros, the transit time effect [27], or frequency dispersion related to extrinsic base surface recombination [28]. This makes the task of finding a precise value for f_T very difficult, especially in the case of state-of-the-art HBT's with cutoff frequencies in excess of 200 GHz. Therefore, a method of characterizing the total delay time based on low frequency measured data would be extremely valuable. In the following, it will be shown that

$$\mathrm{Re}(Z_{22}) \approx \tau_{\mathrm{EC}}/C_{\mathrm{bc}} \quad \text{at low frequencies.} \quad (20)$$

Since C_{bc} is one of those elements which can be evaluated quite precisely at low frequency, the above equation serves as a low frequency rule to find an accurate value of total delay time. In order to prove (20), one needs to consider some "first-order" approximations:

$$\omega C_{\mathrm{bc}} R_{\mathrm{bc}} \gg 1 \quad (21)$$

$$\omega(1-r)^2 C_{\mathrm{bc}} R_{\mathrm{bb}\,i} \ll 1. \quad (22)$$

Equations (21) and (22) are more restrictive than (4)–(6), but one expects them to be still valid for almost an order of magnitude of frequency (typically $1.5\,\mathrm{GHz} \le f \le 15$ GHz). Using assumptions (21) and (11), $\mathrm{Re}(Z_{22})$ can be written as the expression shown at the bottom of the next page, where α_i is the imaginary part of α. Now if one uses the low frequency assump-

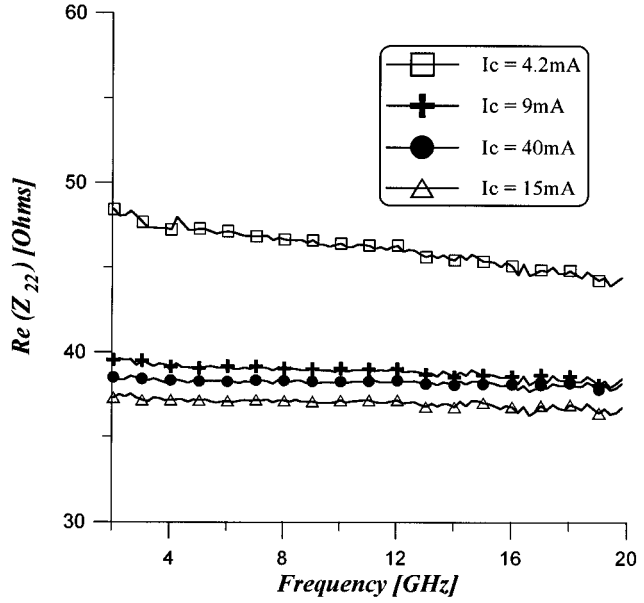

Fig. 8. Variation of $\mathrm{Re}(Z_{22})$ with frequency under various I_c levels. The saturated values of the plots at low frequencies are equal to $\tau_{\mathrm{EC}}/C_{\mathrm{bc}}$. The sudden increase in $\mathrm{Re}(Z_{22})$ at $I_c = 40$ mA is due to the device self-heating (see the text).

tions of $\alpha(\omega)$ (i.e., (16)) and additionally assumes $\alpha_0 \approx 1$, then $\alpha_i \approx -\omega(\tau_B + \tau_C + R_{\mathrm{be}}C_{j\,\mathrm{be}})$ and (20) follows.

Fig. 8 shows the variation of $\mathrm{Re}(Z_{22})$ with frequency for various I_c's. The plot at all different current levels saturate at low frequencies. The constant range of the plots gets narrower for lower current levels, primarily due to the narrower range of validity for assumption (11). The values of τ_{EC} thus calculated are compared in Table I with those obtained from extrapolation of h_{21} at higher frequencies. The slight difference between the two sets of τ_{EC}'s is mainly due to the fact that h_{21} in all of the cases rolls off with gradient less than 20 dB/dec (18.5–19.5 dB/dec in these cases). Therefore, using $\mathrm{Re}(Z_{22})$ is expected to give more accurate delay times. Finally, it should be pointed out that both the above sets of calculated τ_{EC}'s are for the device de-embedded from pad capacitances, which do not belong to the actual device anyway.

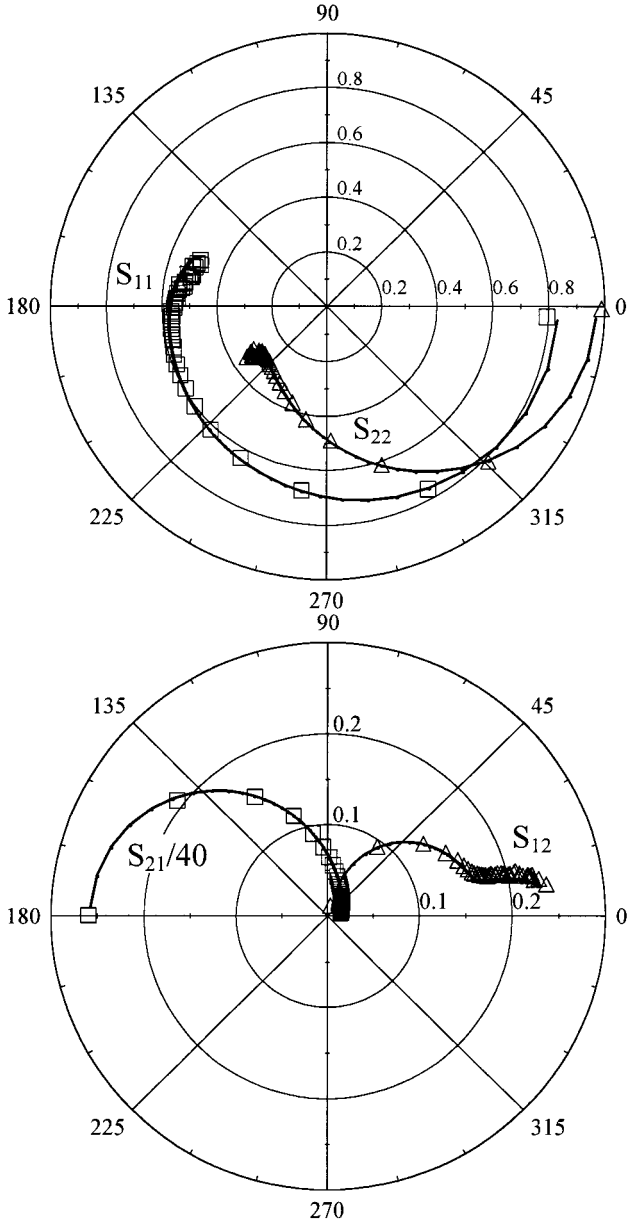

Fig. 9. Comparison between the measured (symbols) and calculated (solid lines) S-parameters at $I_c = 25$ mA and $V_{\mathrm{cb}} = 0.80$ V. Both measured and calculated S_{21} are scaled down by a factor of 40.

V. Discussion

Sections II and III presented a completely analytical HBT parameter extraction technique, which was successfully applied to a $(3\times10)\times4\,\mu\mathrm{m}^2$ InGaP/GaAs DHBT. All the extracted parameters under variable collector current and constant V_{cb} of 0.8 V are summarized in Table I. Fig. 9 compares the measured S-parameters with those calculated using extracted elements at collector current of 25 mA. Excellent agreement between the measured and calculated data can be observed in the entire range

$$\begin{aligned}\mathrm{Re}(Z_{22}) \approx& \mathrm{Re}\left\{\frac{(1-\alpha)[1+j\omega(1-r)C_{\mathrm{bc}}R_{\mathrm{bb}i}]}{j\omega C_{\mathrm{bc}}[1+j\omega r(1-r)C_{\mathrm{bc}}R_{\mathrm{bb}i}]}\right\} + R_{\mathrm{cc}} + R_{\mathrm{ee}} + R_{\mathrm{be}}\\ =& \mathrm{Re}\left\{\frac{(1-\alpha)}{j\omega C_{\mathrm{bc}}} \cdot \frac{[1+j\omega(1-r)C_{\mathrm{bc}}R_{\mathrm{bb}i}]\cdot[1-j\omega r(1-r)C_{\mathrm{bc}}R_{\mathrm{bb}i}]}{1+[\omega r(1-r)C_{\mathrm{bc}}R_{\mathrm{bb}i}]^2}\right\} + R_{\mathrm{cc}} + R_{\mathrm{ee}} + R_{\mathrm{be}}\\ \xrightarrow{(22)} \mathrm{Re}(Z_{22}) \approx& \mathrm{Re}\left\{\frac{(1-\alpha)}{j\omega C_{\mathrm{bc}}}\right\} + R_{\mathrm{cc}} + R_{\mathrm{ee}} + R_{\mathrm{be}} = \frac{-\alpha_i}{\omega C_{\mathrm{bc}}} + R_{\mathrm{cc}} + R_{\mathrm{ee}} + R_{\mathrm{be}}\end{aligned}$$

of frequency. It is known that polar plots of S-parameters do not perfectly reflect the quality of agreement between measured and calculated data. Also the high frequency portion ($f > 10$ GHz) of the S-parameters in a polar plot is compressed in a small area of the plot. Therefore, we have shown the real and imaginary parts of the measured and calculated Z-parameters for $I_c = 9$ mA in Fig. 10(a) and (b), respectively. The calculated Z-parameters also show a very good fit to the measured ones. Excellent agreement between the measured and calculated parameters eliminates the necessity for a final optimization step. Indeed, to prove the latter we have carried out an optimization process using HP-ADS optimization facility with the extracted parameters as initial guess. The values of the elements after optimization for $I_c = 9$ mA are also shown in Table I, together with the average relative errors, as defined in [15], for both calculated and optimized parameters. It is clear that optimization does not improve the error significantly.

Fig. 11 shows the variation of the extracted total B/C junction capacitances in Table I versus collector current. Also shown are the measured capacitances under constant $V_{\rm cb}$ of 0.5 and 1.2 V, and constant $V_{\rm ce}$ of 2.1 V. It can be observed that $C_{\rm bc}$ reduces with increasing I_c under constant $V_{\rm cb}$ condition, similar to the trends observed in [29] and [30]. The reduction of $C_{\rm bc}$ with current is attributed to current-induced broadening of the B/C depletion layer, and the variation of space charge with $V_{\rm cb}$ due to electron velocity modulation [30]. However, all these current dependent phenomena happen inside the intrinsic part of the device where injection of electrons occurs. Therefore, one expects $C_{{\rm bc}x}$ to remain constant, and all the change in $C_{\rm bc}$ should be reflected to a similar change in $C_{{\rm bc}i}$. Consequently, we have chosen to keep $V_{\rm cb}$ constant in our recommended parameter extraction procedure. $C_{{\rm bc}x}$ will be calculated using low current (or cold) measured $C_{\rm bc}$ and $r = (B/E \text{ area})/(B/c \text{ area})$ under the same $V_{\rm cb}$ value as in the high current data; any change in $C_{\rm bc}$ with current will be directly reflected into a similar change in $C_{{\rm bc}i}$ and r. However, one should notice that the variation of r at high current does not change anything in the determination of $R_{{\rm bb}x}$ from cold-HBT data.

Under a constant $V_{\rm ce}$ of 2.1 V, $C_{\rm bc}$ shows an initial increase with I_c. This is due to fact that higher I_c requires higher $V_{\rm be}$, and hence, a lower $V_{\rm cb}$ under constant $V_{\rm ce}$ condition. Therefore, both $C_{{\rm bc}i}$ and $C_{{\rm bc}x}$ will increase initially, and it would be difficult to differentiate between them. Variation of $C_{\rm bc}$ with current under constant $V_{\rm ce}$ was also observed in [15], but the authors did not explain this behavior.

Other interesting features of the data in Table I include a reduction of $R_{{\rm bb}i}$ (and $R_{\rm cc}$ to a smaller extent) at higher currents due to the emitter current crowding. The values of inductances L_b, L_c, and L_e seem to be more or less constant with bias; at highest bias point they all show some increase due to the device self-heating. α_0 shows a continuous increase with collector current and saturates at higher currents before starting to fall-off at the highest bias point. This reflects to a similar trend for the variation of common-emitter dc current gain, β, with current. The sudden change of many of the parameters at $I_c = 40$ mA is most probably due to the device self-heating rather than Kirk effect. Kirk effect (or base push-out) is expected to happen at collector currents around 100 mA for the dimension and collector doping

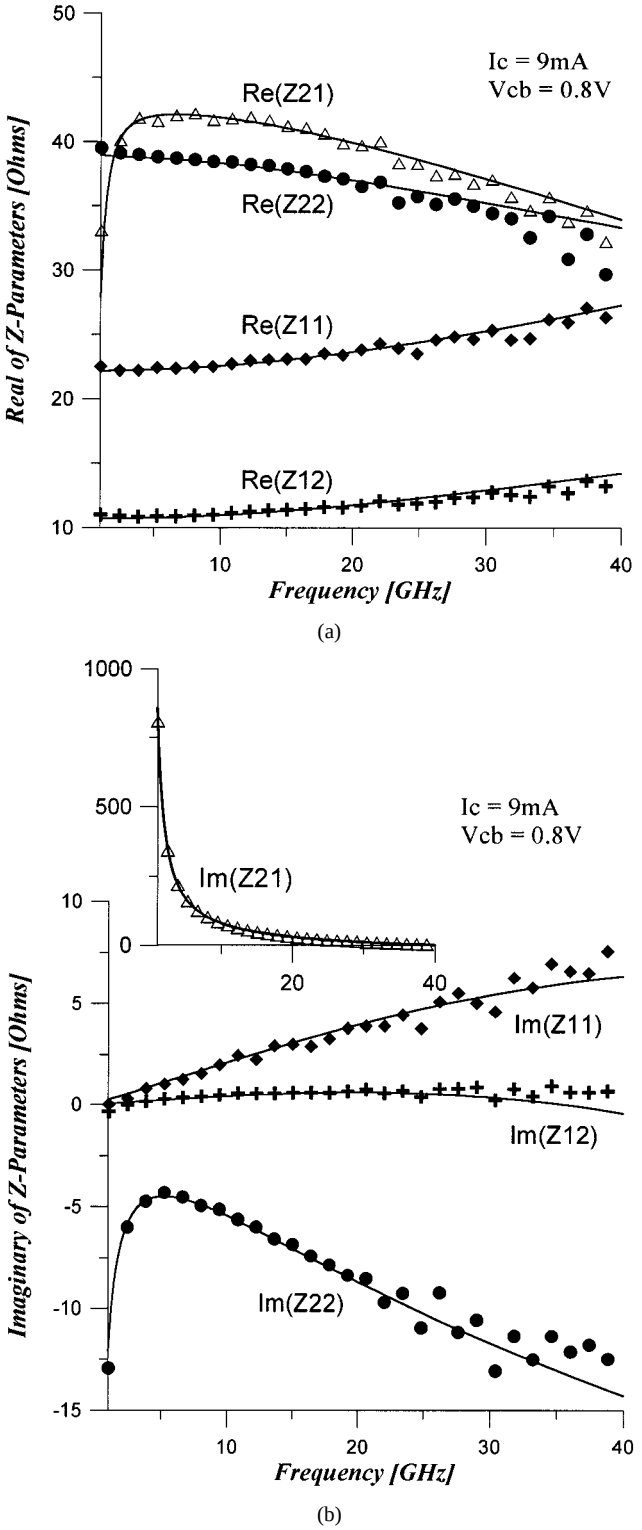

Fig. 10. Comparison between the calculated (solid lines) and measured (symbols): (a) real and (b) imaginary parts of the Z-parameters as a function of frequency under $I_c = 9$ mA and $V_{\rm cb} = 0.80$ V condition. A different I_c level, as compared to Fig. 9, is used to demonstrate the applicability of the present approach for a wide range of bias.

level of the device under study. (See also the following discussion on delay times.) Since device temperature rise is expected to increase both $R_{\rm ee}$ and $R_{\rm be}$ [23], we have evenly divided the sudden increase of $(R_{\rm ee}+R_{\rm be})$ at $I_c = 40$ mA between the two elements.

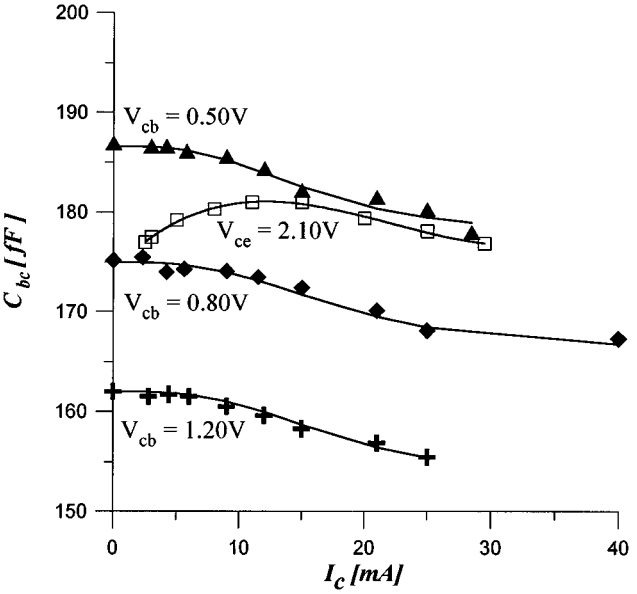

Fig. 11. Extracted values of the total B/C capacitance versus collector current for constant values of $V_{\rm cb}$ (0.50, 0.80, and 1.20 V) and $V_{\rm ce}$ (2.10 V). Solid lines are used just to guide the eyes.

The base transit time remained almost constant (1.61 ± 0.08) ps as the collector current was varied in the range (2–40) mA. This further supports the idea that Kirk effect is not happened at $I_c = 40$ mA. The base transit time can be written as [31]

$$\tau_B = \frac{W_B^2}{2D_{nB}} + \frac{W_B}{v_{n,\rm avrg.}} \tag{23}$$

where W_B is the neutral base width, D_{nB} is the diffusion constant in the base, and $v_{n,\rm avrg.}$ is an average velocity of electrons at the base end of the B/C depletion region. $v_{n,\rm avrg.}$ is higher than the static saturation velocity of electrons due to the velocity overshoot effect. We adopt 2.05×10^7 cm/s for the latter parameter as in [23]. For the base doping density in the present device, minority electron mobility of $\sim$2000 cm^2/V·s is expected [32] which results in $D_{nB} \approx 50$ cm^2/s. Therefore, using $W_B \approx 900$ Å one obtains $\tau_B = 1.25$ ps from (23). The larger measured value of τ_B is due to the carrier trapping behind the triangular potential barrier at the B/C heterojunction, as discussed in [5]. Also, since minority electron mobility inside the base varies with temperature as $1/T$ [33], D_{nB} will be almost temperature independent. Consequently, τ_B does not change significantly as self-heating occurs, though it may change slightly through the reduction of $v_{n,\rm avrg.}$.

The collector depletion layer delay time can also be expressed as $\tau_C = W_{\rm BC}/2v_{n,\rm avrg.}$, where $W_{\rm BC}$ is the B/C depletion layer width (Fig. 1). $W_{\rm BC}$ can be estimated using $C_{\rm bc} = 175$ fF as $\sim$0.19 μm. Therefore, average value of τ_C at low current levels $(0.79 \pm 0.07$ ps) results in $v_{n,\rm avrg.} \approx 1.2 \times 10^7$ cm/s inside InGaP collector, which is supposed to be somewhat smaller than the average velocity of electrons inside GaAs [5]. When self-heating occurs, this velocity is expected to be significantly reduced [23], hence causing a sharp increase of τ_C under high current condition. The increase of $R_{\rm be}$, $R_{\rm cc}$, and $R_{\rm ee}$ with temperature are other contributors to the enlargement of $\tau_{\rm EC}$ at the highest current level in Fig. 5. The y-intercept of the linear fit to the low current variation of $\tau_{\rm EC}$ with $(1/I_c)$ is 5.65 ps $(=\tau_F + (R_{\rm ee} + R_{\rm cc})C_{\rm bc})$. Using average values of $R_{\rm ee}$, $R_{\rm cc}$, and $C_{\rm bc}$ in Table I, the term $(R_{\rm ee} + R_{\rm cc})C_{\rm bc}$ can be calculated as 3.35 ps, which results in $\tau_F \approx 2.30$ ps. This is close, but not exactly equal, to the y-intercept of $(\tau_F + R_{\rm be}C_{j\,\rm be})$ versus $(1/I_c)$, which is 2.41 ps. As discussed in Section IV, the latter method is expected to give more accurate values of τ_F.

VI. Conclusion

In this work, an improved HBT small-signal parameter extraction technique is developed and applied to extract the parameters of an InGaP/GaAs DHBT. The method relies on measurement of S-parameters under constant $V_{\rm cb}$ but variable I_c, including cold-HBT $(I_c = 0)$ measurement. The approximations used to derive the simplified Z-parameter formulations were revised, and it was shown that the present method benefits from a wide range of applicability, which makes it appropriate for various types of HBT's including InP-based and GaAs-based single and double HBT's. Furthermore, all equivalent circuit elements are extracted directly without reference to numerical optimization, and it was shown that an optimization step following the analytical extraction does not improve the error significantly. Therefore, we believe that this method can be used as a standard technique to extract the equivalent circuit elements of various types of HBT's. We have also applied the above parameter extraction technique to InP-based HBT's, results of which will be presented in a forthcoming publication.

In addition, it was shown in Section IV that for the device de-embedded from parasitic pad capacitances $\mathrm{Re}(Z_{22}) \approx \tau_{\rm EC}/C_{\rm bc}$ at low frequencies. Therefore, total delay time of an HBT can be extracted at low frequencies, without the need to measure h_{21} at very high frequencies and/or extrapolate h_{21} with -20 dB/dec roll-off. Furthermore, the methods presented in [5] and [25] for extracting the forward transit time was modified to evaluate τ_F and its components (τ_B and τ_C) more accurately.

Analysis of the extracted elements in Section V demonstrated that all of them behave according to physical expectations. Among the physical phenomena observed and explained were the reduction of B/C junction capacitance at high collector currents, the effect of self-heating on small-signal elements and delay times, and reduction of $R_{{\rm bb}\,i}$ and $R_{\rm cc}$ due to emitter current crowding.

Appendix
Z-Parameter Relations

Consider the HBT small-signal equivalent circuit shown in Fig. 1. After de-embedding the parasitic pad capacitances and merging $R_{{\rm cc}\,i}$ and $R_{{\rm cc}\,x}$ into a single element $R_{\rm cc}$, as discussed in Section II, one can arrive at the following Z-parameter relations:

$$Z_{11} = \frac{R_{{\rm bb}\,i}[(1-\alpha)Z_{{\rm bc}\,i} + Z_{{\rm bc}\,x}]}{R_{{\rm bb}\,i} + Z_{{\rm bc}\,i} + Z_{{\rm bc}\,x}} + Z_B + Z_E \tag{A1a}$$

$$Z_{12} = \frac{(1-\alpha)R_{{\rm bb}\,i}Z_{{\rm bc}\,i}}{R_{{\rm bb}\,i} + Z_{{\rm bc}\,i} + Z_{{\rm bc}\,x}} + Z_E \tag{A1b}$$

$$Z_{21} = \frac{[(1-\alpha)R_{\mathrm{bb}\,i} - \alpha Z_{\mathrm{bc}\,x}]Z_{\mathrm{bc}\,i}}{R_{\mathrm{bb}\,i} + Z_{\mathrm{bc}\,i} + Z_{\mathrm{bc}\,x}} + Z_E \tag{A1c}$$

$$Z_{22} = \frac{(1-\alpha)Z_{\mathrm{bc}\,i}(R_{\mathrm{bb}\,i} + Z_{\mathrm{bc}\,x})}{R_{\mathrm{bb}\,i} + Z_{\mathrm{bc}\,i} + Z_{\mathrm{bc}\,x}} + Z_C + Z_E \tag{A1d}$$

Therefore

$$Z_{11} - Z_{12} = \frac{R_{\mathrm{bb}\,i}Z_{\mathrm{bc}\,x}}{R_{\mathrm{bb}\,i} + Z_{\mathrm{bc}\,i} + Z_{\mathrm{bc}\,x}} + Z_B \tag{A2a}$$

$$Z_{22} - Z_{21} = \frac{Z_{\mathrm{bc}\,i}Z_{\mathrm{bc}\,x}}{R_{\mathrm{bb}\,i} + Z_{\mathrm{bc}\,i} + Z_{\mathrm{bc}\,x}} + Z_C \tag{A2b}$$

$$Z_{12} - Z_{21} = \frac{\alpha Z_{\mathrm{bc}\,i}Z_{\mathrm{bc}\,x}}{R_{\mathrm{bb}\,i} + Z_{\mathrm{bc}\,i} + Z_{\mathrm{bc}\,x}}. \tag{A2c}$$

The impedance blocks in equations (A1) and (A2) are defined (see also Fig. 1) as

$$Z_{\mathrm{bc}\,i} = \frac{R_{\mathrm{bc}\,i}}{1 + j\omega C_{\mathrm{bc}\,i}R_{\mathrm{bc}\,i}} \tag{A3}$$

$$Z_{\mathrm{bc}\,x} = \frac{R_{\mathrm{bc}\,x}}{1 + j\omega C_{\mathrm{bc}\,x}R_{\mathrm{bc}\,x}} \tag{A4}$$

$$Z_E = R_{\mathrm{ee}} + j\omega L_e + \frac{R_{\mathrm{be}}}{1 + j\omega C_{\mathrm{be}}R_{\mathrm{be}}} \tag{A5}$$

$$Z_B = R_{\mathrm{bb}\,x} + j\omega L_b \tag{A6}$$

$$Z_C = R_{\mathrm{cc}} + j\omega L_c \tag{A7}$$

The common-base current gain $\alpha(\omega)$ and the input capacitance C_{be} can also be written as [16], [17]:

$$\alpha(\omega) = \frac{\alpha_0 \cdot \exp[-j\omega((1-m)\tau_B + \tau_C)]}{1 + j\omega C_{\mathrm{be}}R_{\mathrm{be}}} \cdot \frac{\sin(\omega\tau_C)}{\omega\tau_C} \tag{A8}$$

$$C_{\mathrm{be}} = C_{j\,\mathrm{be}} + \frac{m\tau_B}{R_{\mathrm{be}}} \tag{A9}$$

where

- α_0 common-base dc current gain;
- τ_B base transit time;
- τ_C collector depletion region delay time;
- m empirical factor that fits the single-pole expression of base transport factor to its more accurate secant hyperbolic representation [16].

A value of $m \approx 5/6$ is used in the majority of the previous publications. C_{be} includes the terms related to both B/E depletion capacitance and the so-called base diffusion (or storage) capacitance.

ACKNOWLEDGMENT

The authors would like to thank K. Smith for technical assistance, and A. Lai for optimization of parameters. M. Sotoodeh also wishes to acknowledge the scholarship provided by the Ministry of Culture and Higher Education (MCHE) of Iran.

REFERENCES

[1] B. Bayraktaroglu, "GaAs HBT's for microwave integrated circuits," *Proc. IEEE*, vol. 81, pp. 1762–1785, Dec. 1993.

[2] P. M. Asbeck *et al.*, "GaAs-based heterojunction bipolar transistors for very high performance electronic circuits," *Proc. IEEE*, vol. 81, pp. 1709–1726, Dec. 1993.

[3] D. Costa, W. U. Liu, and J. S. Harris Jr., "Direct extraction of the AlGaAs/GaAs heterojunction bipolar transistor small-signal equivalent circuit," *IEEE Trans. Electron Devices*, vol. 38, pp. 2018–2024, Sept. 1991.

[4] D. R. Pehlke and D. Pavlidis, "Evaluation of the factors determining HBT high-frequency performance by direct analysis of S-parameter data," *IEEE Trans. Microwave Theory Tech.*, vol. 40, pp. 2367–2373, Dec. 1992.

[5] M. Sotoodeh *et al.*, "Direct extraction and numerical simulation of the base and collector delay times in double heterojunction bipolar transistors," *IEEE Trans. Electron Devices*, vol. 46, pp. 1081–1086, June 1999.

[6] C.-J. Wei and J. C. M. Hwang, "Direct extraction of equivalent circuit parameters for heterojunction bipolar transistors," *IEEE Trans. Microwave Theory Tech.*, vol. 43, pp. 2035–2040, Sept. 1995.

[7] A. Samelis and D. Pavlidis, "DC to high-frequency HBT-model parameter evaluation using impedance block conditioned optimization," *IEEE Trans. Microwave Theory Tech.*, vol. 45, pp. 886–897, June 1997.

[8] S. J. Spiegel, D. Ritter, R. A. Hamm, A. Feygenson, and P. R. Smith, "Extraction of the InP/GaInAs heterojunction bipolar transistor small-signal equivalent circuit," *IEEE Trans. Electron Devices*, vol. 42, pp. 1059–1064, June 1995.

[9] U. Schaper and B. Holzapfl, "Analytical parameter extraction of the HBT equivalent circuit with T-like topology from measured S-parameters," *IEEE Trans. Microwave Theory Tech.*, vol. 43, pp. 493–498, Mar. 1995.

[10] J. M. M. Rios, L. M. Lunardi, S. Chandrasekhar, and Y. Miyamoto, "A self-consistent method for complete small-signal parameter extraction of InP-based heterojunction bipolar transistors (HBT's)," *IEEE Trans. Microwave Theory Tech.*, vol. 45, pp. 39–45, Jan. 1997.

[11] A. Kameyama, A. Massengale, C. Dai, and J. S. Harris Jr., "Analysis of device parameters for pnp-type AlGaAs/GaAs HBT's including high-injection using new direct parameter extraction," *IEEE Trans. Electron Devices*, vol. 44, pp. 1–10, Jan. 1997.

[12] G. Dambrine, A. Cappy, F. Heliodore, and E. Playez, "A new method for determining the FET small-signal equivalent circuit," *IEEE Trans. Microwave Theory Tech.*, vol. 36, pp. 1151–1159, July 1988.

[13] M. Berroth and R. Bosch, "Broad-band determination of the FET small-signal equivalent circuit," *IEEE Trans. Microwave Theory Tech.*, vol. 38, pp. 891–895, July 1990.

[14] B. Li and S. Prasad, "Basic expressions and approximations in small-signal parameter extraction for HBT's," *IEEE Trans. Microwave Theory Tech.*, vol. 47, pp. 534–539, May 1999.

[15] B. Li, S. Prasad, L.-W. Yang, and S. C. Wang, "A semianalytical parameter-extraction procedure for HBT equivalent circuit," *IEEE Trans. Microwave Theory Tech.*, vol. 46, pp. 1427–1435, Oct. 1998.

[16] R. L. Pritchard, *Electrical Characteristics of Transistors*. New York: McGraw Hill, 1967.

[17] W. Liu, *Handbook of III–V Heterojunction Bipolar Transistors*. New York: Wiley, 1998.

[18] Y. Gobert, P. J. Tasker, and K. H. Bachem, "A physical, yet simple, small-signal equivalent circuit for the heterojunction bipolar transistor," *IEEE Trans. Microwave Theory Tech.*, vol. 45, pp. 149–153, Jan. 1997.

[19] M. Vaidyanathan and D. L. Pulfrey, "Extrapolated $f_{\max}$ of heterojunction bipolar transistors," *IEEE Trans. Electron Devices*, vol. 46, pp. 301–309, Feb. 1999.

[20] R. Anholt *et al.*, "Measuring, modeling, and minimizing capacitances in heterojunction bipolar transistors," *Solid-State Electron.*, vol. 39, pp. 961–963, July 1996.

[21] A. H. Khalid, M. Sotoodeh, and A. A. Rezazadeh, "Planar self-aligned microwave InGaP/GaAs HBT's using He^+/O^+ implant isolation," in *Proc. 5th Int. Workshop High Performance Electron Devices for Microwave and Optoelectronic Applications* , 1997, pp. 279–284.

[22] I. E. Getreu, *Modeling the Bipolar Transistor*. New York: Elsevier, 1978.

[23] D. A. Ahmari *et al.*, "Temperature dependence of InGaP/GaAs heterojunction bipolar transistor DC and small-signal behavior," *IEEE Trans. Electron Devices*, vol. 46, pp. 634–640, Apr. 1999.

[24] S. Lee, "Effects of pad and interconnection parasitics on forward transit time in HBT's," *IEEE Trans. Electron Devices*, vol. 46, pp. 275–280, Feb. 1999.

[25] ——, "Forward transit time measurement for heterojunction bipolar transistors using simple Z parameter equation," *IEEE Trans. Electron Devices*, vol. 43, pp. 2027–2029, Nov. 1996.

[26] W. Liu, D. Costa, and J. S. Harris Jr., "Derivation of the emitter-collector transit time of heterojunction bipolar transistors," *Solid-State Electron.*, vol. 35, pp. 541–545, Apr. 1992.
[27] S. Prasad, W. Lee, and C. G. Fonstad, "Unilateral gain of heterojunction bipolar transistors at microwave frequencies," *IEEE Trans. Electron Devices*, vol. 35, pp. 2288–2294, Dec. 1988.
[28] B. Ihn *et al.*, "Surface recombination related frequency dispersion of current gain in AlGaAs/GaAs HBTs," *Electron. Lett.*, vol. 34, pp. 1031–1033, 1998.
[29] L. H. Camnitz and N. Moll, "An analysis of the cutoff-frequency behavior of microwave heterostructure bipolar transistors," in *Compound Semiconductor Transistors: Physics and Technology*, S. Tiwari, Ed. Piscataway, NJ: IEEE Press, 1993, pp. 21–45.
[30] Y. Betser and D. Ritter, "Reduction of the base-collector capacitance in InP/GaInAs heterojunction bipolar transistors due to electron velocity modulation," *IEEE Trans. Electron Devices*, vol. 46, pp. 628–633, Apr. 1999.
[31] M. B. Das, "High-frequency performance limitations of millimeter-wave heterojunction bipolar transistors," *IEEE Trans. Electron Devices*, vol. 35, pp. 604–614, May 1988.
[32] S. Adachi, *GaAs and Related Materials: Bulk Semiconducting and Superlattice Properties*, Singapore: World Scientific, 1994, p. 602.
[33] K. Beyzavi *et al.*, "Temperature dependence of minority-carrier mobility and recombination time in p-type GaAs," *Appl. Phys. Lett.*, vol. 58, no. 12, pp. 1268–1270, 1991.

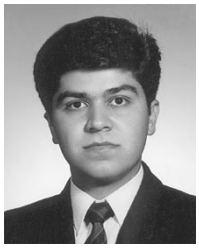

Mohammad Sotoodeh was born in 1968. He received the B.Sc. and M.Sc. degrees (with highest honors), both in electronic engineering, from Isfahan University of Technology, Iran, and from the University of Tehran, Iran in 1991 and 1994, respectively. He is currently pursuing the Ph.D. degree at King's College London, U.K. His research thesis is on design, optimization, and characterization of InGaP/GaAs double HBT's for microwave power applications.

His research interests include heterojunction bipolar transistors for high frequency, high power, and/or high temperature applications, numerical simulation of semiconductor devices, dc and high frequency characterization of HBT's, III–V semiconductor compounds and their material parametrization.

Mr. Sotoodeh is the winner of the first award in the third Nationwide Olympiad of Mathematics held in Zahedan, Iran, in 1986.

Lucia Sozzi was born in Piacenza, Italy, in 1974. She is currently pursuing the Laurea degree in electronic engineering at the University of Parma, Parma, Italy. During her final year's project she spent a research leave with the Department of Electronic Engineering, King's College London, U.K., where she worked on HBT, rf, and dc modeling and characterization.

Alessandro Vinay was born in Piacenza, Italy, in 1973. He is currently pursuing the Laurea degree in electronic engineering at the University of Parma, Parma, Italy. During his final year's project he spent a research leave with the Department of Electronic Engineering, King's College London, U.K., working on HBT modeling and characterization.

A. H. Khalid received the M.Sc. degree in physics from Government College, Lahore, Pakistan, and the M.Phil. degree in experimental semiconductor physics in 1990 from Quaid-i-Azam University, Islamabad, Pakistan.

He joined the Department of Electronics, Quaid-i-Azam University, as a Research Associate, to characterize the conductive polymers. In 1992, he registered for the Ph.D. at King's College, London, U.K. His research work was on fabrication and design of transparent gate field effect transistors (TGFET's). He then worked on EPSRC funded projects on fabrication of multilayer MMIC's on GaAs substrate. He also worked on fabrication of self-aligned double heterostructure bipolar transistors (DHBT's). His research interests are in material properties of indium-tin oxide (ITO) and ITO-based contact technology, and novel fabrication techniques for advanced semiconductor devices such as HEMT's and HBT's. He is currently with King's College.

Zhirun Hu received the B.Eng. degree in telecommunication engineering from Nanjing Institute of Posts and Telecommunications, Nanjing, China, in 1982, and the M.B.A. degree and Ph.D. degree in electrical and electronic engineering from the Queen's University of Belfast, Belfast, U.K., in 1988 and 1991, respectively.

In 1991, he joined the Department of Electrical and Electronic Engineering, University College of Swansea, U.K., as a Senior Research Assistant in semiconductor device simulation. In 1994, he rejoined the Department of Electrical and Electronic Engineering, Queen's University of Belfast, as a Research Fellow in silicon MMIC design. In 1996, he joined GEC Marconi Instruments as a Microwave Technologist working on the new generation of microwave power detector/sensors. He is presently a Lecturer in the Department of Electronic Engineering, King's College, University of London. His main research interests include computer-aided design and optimization of microwave and millimeter-wave integrated circuits, artificial neural network modeling for passive 3-D microwave components, and wide-band gap heterojunction device simulation and optimization.

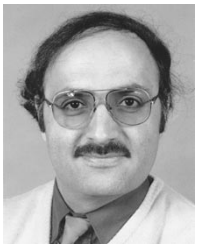

Ali Rezazadeh (M'91) received the Ph.D. degree in applied solid state physics from the University of Sussex, Brighton, U.K., in 1983.

In September 1983, he joined GEC-Marconi Hirst Research Centre as a Research Scientist and became the Group Leader responsible for research and development into advanced HBT devices and circuits for high-speed and digital applications. In 1988, he became a Senior Research Associate-Group Leader responsible for research and development into advanced high electron mobility transistor devices and circuits for analogue applications. In October 1990, he joined the academic staff of the Department of Electronic Engineering at King's College, London. He is currently a Reader in Microwave Photonics and Consulting Engineer in the Department of Electronic Engineering, King's College. He is also the Head of Microwave Circuits and Devices Research Group, one of the four research groups in the department. His present work involves the physics and technology of III–V heterojunction devices and circuits for microwave and optoelectronic applications. He has contributed three chapters of books and produced 40 refereed journal papers and 50 conference papers.

Dr. Rezazadeh is the Chairman of IEEE UK&RI MTT/ED/AP/LEO Joint Chapter and the Chairman of IEE Professional Group E3 (Microelectronics and Semiconductor Devices). He also serves on the Technical Committees of several international conferences. In 1993, he founded The IEEE International Symposium on Electron Devices for Microwave and Optoelectronic Applications (EDMO).

Roberto Menozzi was born in Genova, Italy, in 1963. He received the Laurea degree (cum laude) in electronic engineering from the University of Bologna, Bologna, Italy, in 1987, and the Ph.D. degree in information technology from the University of Parma, Parma, Italy, in 1994.

After serving in the army, he joined a research group at the Department of Electronics, University of Bologna, Bologna, Italy. Since 1990, he has been with the Department of Information Technology, University of Parma, where he became Research Associate in 1993 and Associate Professor in 1998. His research activities have covered the study of latch-up in CMOS circuits, IC testing, power diode physics, modeling and characterization, and the dc, rf, and noise characterization, modeling, and reliability evaluation of compound semiconductor and heterostructure electron devices such as MESFET's, HEMT's, HFET's, and HBT's.